Electronic Supplementary Material (ESI) for RSC Applied Polymers.
This journal is © The Royal Society of Chemistry 2024

Supplementary Information

Preparation of gradient porous polymer membranes with multifunctionality

Weigang Ji, Xiaohu Li, Qi Xi, Mengyuan Song, Xue Wu, Pengfei Song*

College of Chemistry and Chemical Engineering, Key Laboratory of Eco-functional Polymer Materials of the Ministry of Education, Key Laboratory of Eco-environmental Polymer Materials of Gansu Province, Gansu International Scientific and Technological Cooperation Base of Water-Retention Chemical Functional Materials, Northwest Normal University, Lanzhou 730070, China

* Corresponding Emails: songpf@nwnu.edu.cn

Contents

2. EXPERIMENTAL SECTION

2.1 Materials.

(±)-α-Lipoic acid, 1-Vinylimidazole, bromoacetonitrile, azodiisobutyronitrile, bis-(trifluoromethane sulfonyl)imide lithium salt were purchased from Energy Chemical. Dimethyl sulfoxide (DMSO), tetrahydrofuran (THF), and ethanol were purchased from Beijing Chemicalworks. All the other chemical reagents were of analytical grade and used as received.

2.2 Preparation of PCMVImTf_2N [1]

In a 100 mL flask, 1-vinylimidazole (5 g, 0.053 mol) and bromoacetonitrile (6.3 g, 0.053 mol) were added to 35 mL of acetone. The mixture was stirred at room temperature for 24 h. The precipitate was filtered out and washed with ether and finally dried under vacuum at room temperature for 24 h. The precipitate was filtered out and washed with ether and finally dried under vacuum at room temperature to yield 1-cyanomethyl-3-vinylimidazole bromide. 10 g 1-cyanomethyl-3-vinylimidazole bromide monomer, 0.2 g AIBN and 100 ml dimethyl sulfoxide were packed into a 250 ml flask. The mixture was deoxygenated three times by a freeze pump-thaw procedure and finally charged with nitrogen. The reaction mixture was then placed in an oil bath at 80°C for 24 hours. When cooled to room temperature, the reaction mixture is added drop by drop to an excess of THF. The precipitate was filtered off, washed with excess ethanol and dried under vacuum at 60°C to obtain PCMVImBr. 10 g of PCMVImBr was dissolved in 200 ml of deionized water. A 100 ml aqueous solution of 13 g bis(trifluoromethane sulfonyl)imide lithium salt was added dropwise to the aqueous solution of PCMVImBr. After addition, the reaction mixture was allowed to stir for 2 h. The precipitate was collected by filtration, washed several times with deionized water and dried under vacuum at 60°C.

2.3 Preparation of PIL/PTA membrane.

Typically, the preparation process of PIL/PTA-5 is used as an example. 0.21 g of lipoic acid and 0.39 g of PCMVImTf_2N were weighed and dissolved in 5 mL of ethanol and 2 mL of DMSO, respectively. The two solutions were then mixed at room temperature and stirred until homogeneous. The resulting homogeneous solution was poured into the abrasive tool, spread all over the bottom, transferred to a vacuum oven at 80°C and heated for 4 h. After it cooled to room temperature, the polymer-attached mould was immersed in 0.2 wt% ammonia for 5 h to obtain a porous membrane, washed with water several times, and stored in a wet condition before use.

2.4 Characterizations.

^{1}H and ^{13}C NMR spectra were recorded on a Bruker AV 300 or Bruker AM 600 in solvents as indicated. Chemical shifts (δ) for ^{1}H and ^{13}C NMR spectra are given in ppm relative to TMS. Variable-Temperature Fourier transform infrared spectroscopy (FT-IR) spectra were accomplished on a Brucker IFS66V FT-IR spectrometer the sample was dried at 60 ℃. Raman spectroscopy of freeze-dried PIL-PTA membranes was acquired using Raman imaging system (LabRam HR Evolution) on the range of 1000–300 cm^{-1}. The morphologies of the PIL-PTA membranes were freeze-dried and viewed by field-emission scanning electron microscopy (SEM and EDS, ULTRA Plus, Zeiss); samples were coated with a thin layer of gold before examination. Thermogravimetric analysis was carried out on a NETZSCH STA 409PC instrument under purified nitrogen gas flow at 10 °C min^{-1}. The tensile tests of the PIL-PTA membranes were recorded by dynamic mechanical analysis (EZ-Test, SHIMADZU) at a strain rate of 10 mm/min. The UV−vis absorbance data of the resulted samples were tested by using the UV−vis spectrophotometer (Shimadzu UV-3600 Plus). The change electrochemical resistance of the PIL-PTA membranes was determined by an electrochemical workstation (CHI760E, Shanghai Chenhua Instrument Co., Ltd) with a three-electrode system. The relative resistance change of the PIL-PTA membranes was obtained as follows:

$$\Delta R/R_0 = (R - R_0)/R_0$$

where R_0 is the resistance without strain and R denotes the real-time resistance.

2.5 Bending/de-bending experiments of PIL/PTA membranes under acetone stimulation.

We tested the bending/de-bending performance of the porous membrane stimulated by acetone vapor and acetone solvent, respectively. Then a piece of membrane strip (30mm*2mm) was placed place it in acetone vapor or solvent (atmospheric pressure, 20℃); the solvent vapor（solvent）will trigger the fast bending movement. Record the time required for the porous membrane from contacting acetone vapor (solvent) to completing deformation. Afterwards, the membrane was pulled back into air to accomplish the shape recovery. In the bending/de-bending experiments in acetone vapor, we measured the effect of the monomer mass ratio in PIL/PTA on the stimulus response performance by calculating the curvature.

In solvent sensing testing, PIL/PTA-5 membrane are clamped at both ends of the electrode of

the electrochemical workstation, and acetone solutions of different concentrations are dropped onto PIL/PTA-5 membrane in equal volume from low to high concentrations. The electrochemical workstation records the changes in resistance values under different conditions.

2.6 Self-healing test.

The PIL/PTA membranes was cut into two piece of membrane strip by a knife, and the interfaces were contacted on an arbitrarily flat surface. A drop of acetone is placed on the cut and kept it still for 10 min to ensure that the acetone completely evaporates in the air. The acetone stimulated bending/debonding experiment was then repeated with the membrane.

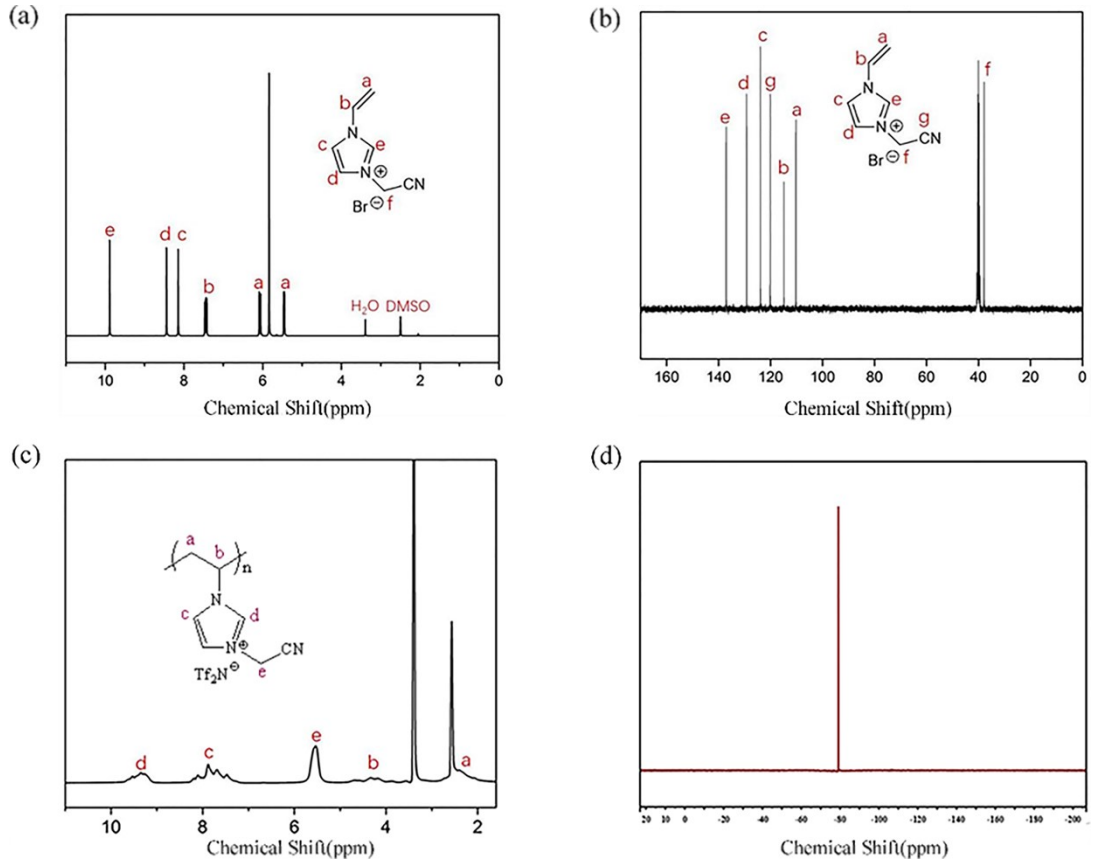

Fig. S1. (a) ^{1}H NMR spectrum of 1-cyanomethyl-3-vinylimidazolium bromide. (b) ^{13}C NMR spectrum of 1-cyanomethyl-3-vinylimidazolium bromide. (c) ^{1}H NMR spectrum of poly[3-cyanomethyl-1-vinylimidazolium bis(trifluoromethane sulfonyl)imide]. (d) ^{19}F NMR spectrum of poly[3-cyanomethyl-1-vinylimidazolium bis(trifluoromethane sulfonyl)imide].

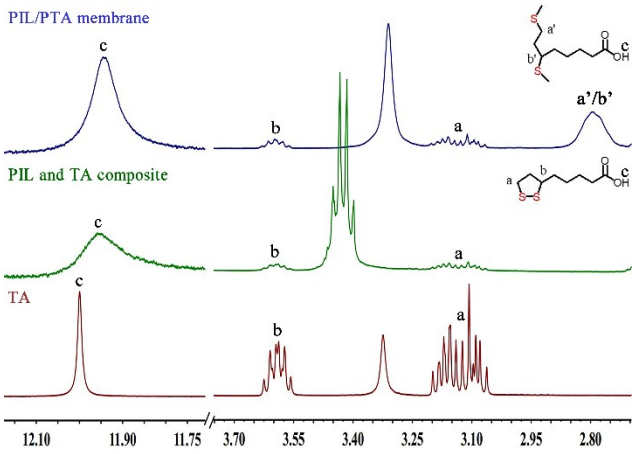

Fig. S2. ^{1}H NMR spectrum comparison among TA powder, PIL and TA composite and PIL/PTA membrane. (^{1}H NMR spectrum of PIL/PTA membrane appeared a signal at 2.81 ppm is assigned to PTA, indicating the ring-opening polymerization of TA in the solution blending process. Moreover, the resonance signal peak of COOH in TA shifts from 12.03 to 11.96 ppm in the ionogel, which also proves the hydrogen bond effect between PIL network and PTA.)

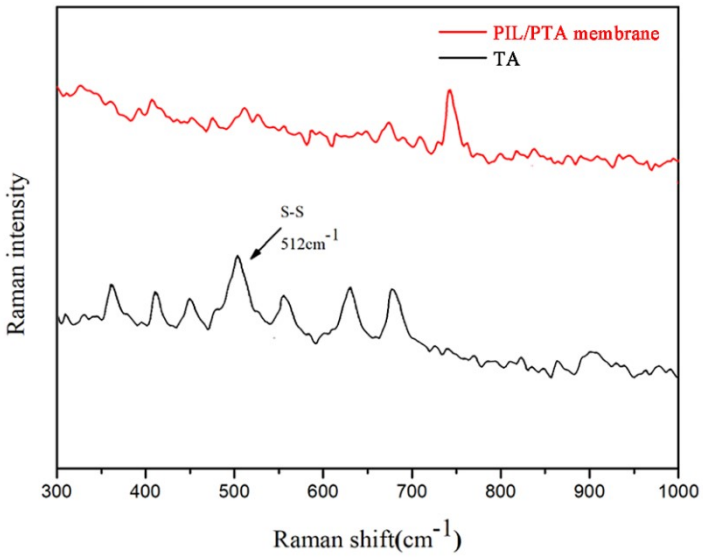

Fig. S3. Raman spectrum of TA powder and PIL/PTA membrane. The peak of disulfide bond at 513cm^{-1} of TA almost disappeared in the PIL/PTA membrane, which proved the polymerization process of TA.

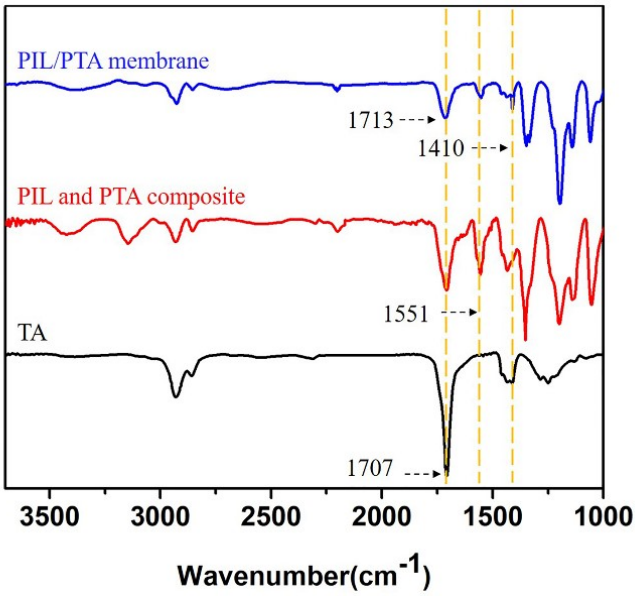

Fig. S4. FT-IR spectra comparison among TA powder, PIL and PTA composite and PIL/PTA membrane. FTIR spectra of PIL/PTA membrane showed the characteristic absorption peak at 1551 cm^{-1} and 1410cm^{-1} stretching are assigned to COO^- NH_4^+ groups. The shift of C=O peak from 1707 cm^{-1} to 1713cm^{-1} and the appearance of a new peak at 3439 cm^{-1} indicate that hydrogen bonding is formed in the polymer chain.

Table S1. Preparation of gradient porous membranes with different TA content.

Sample	PCMVImTf_2N/g	TA/g	Thickness /mm
PIL/PTA -1	0.15	0.45	0.223
PIL/PTA-2	0.21	0.39	0.230
PIL/PTA -3	0.27	0.33	0.225
PIL/PTA -4	0.33	0.27	0.233
PIL/PTA-5	0.39	0.21	0.236

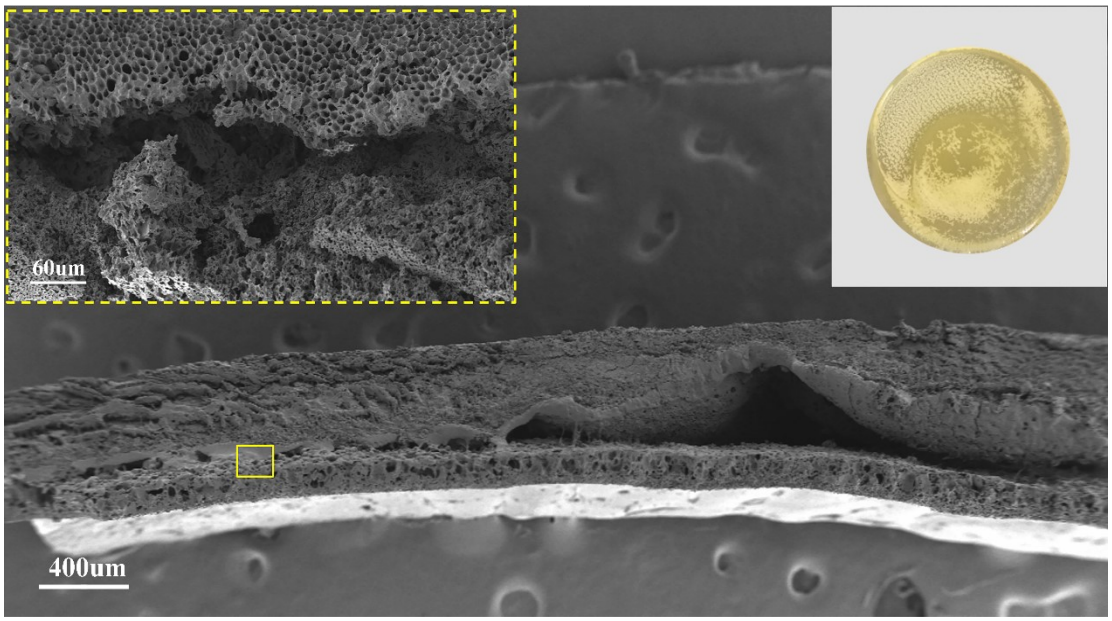

Fig. S5. SEM images of the cross-section of the PCMVImBr/PTA membrane. Inset is an electron micrographs of the PCMVImBr/PTA membrane and SEM image of the region marked with a yellow box.

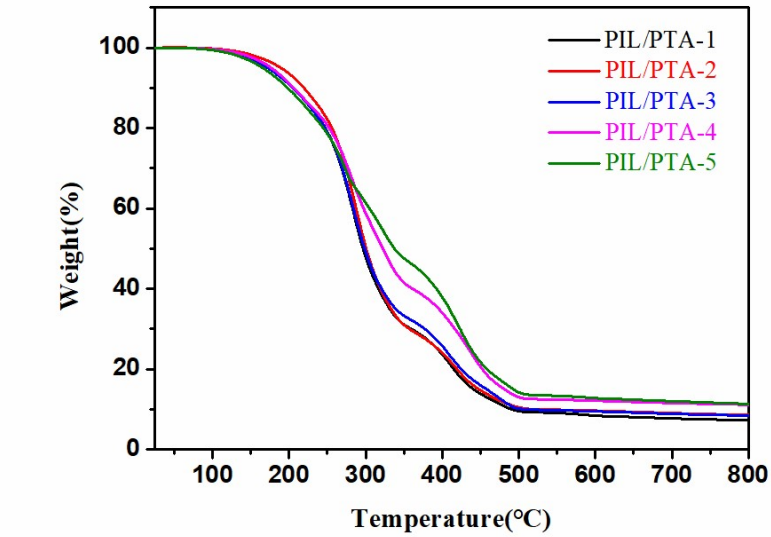

Fig. S6. Thermal analysis of PIL/PTA membranes. The 5% weight loss temperature is over 200 ℃ and the maximum weight loss temperature is 300 ℃.

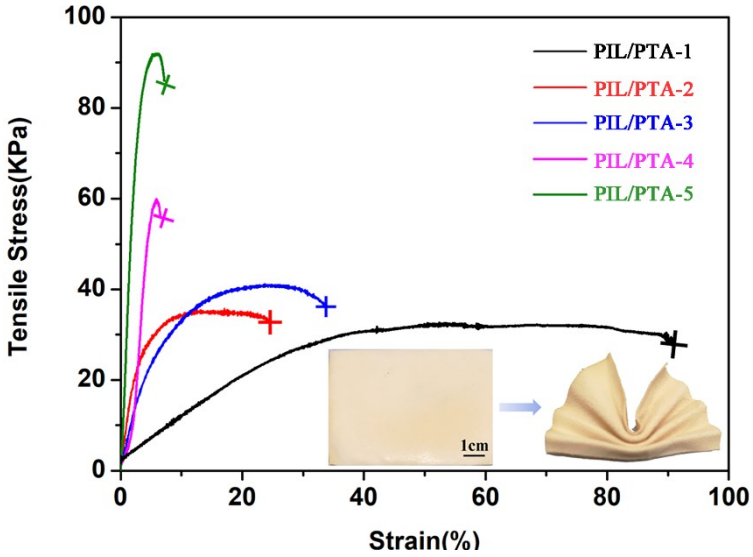

Fig. S7. Tensile stress curve of PIL/PTA membrane. The inset photograph shows the PIL/PTA-5 membrane folded into sectors.

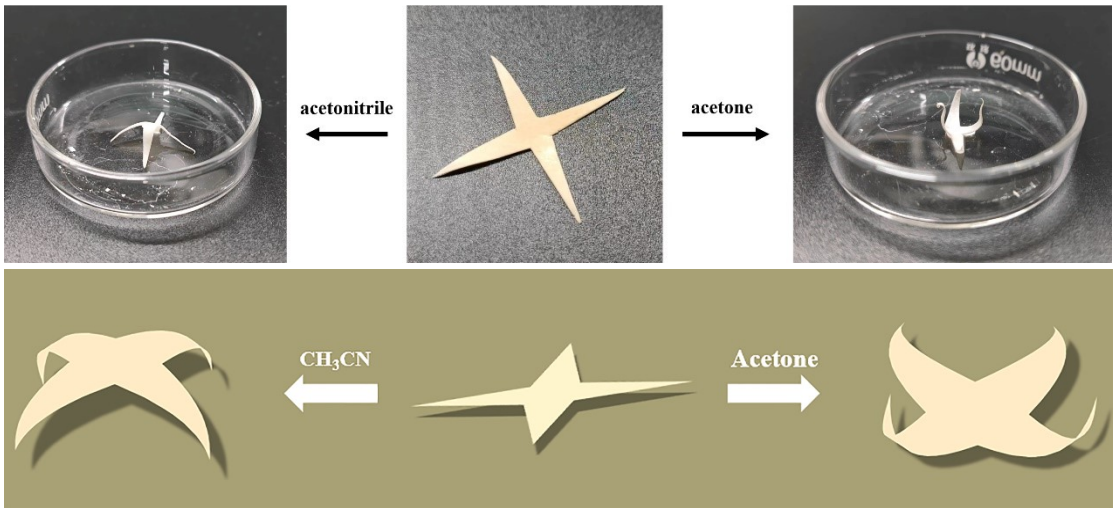

Fig. S8. Digital photograph and Schematic illustration of PIL/PTA-5 membrane recognition acetonitrile or acetone. (PIL/PTA-5 membrane bends toward the "top" in acetone and toward the "bottom" in acetonitrile.)

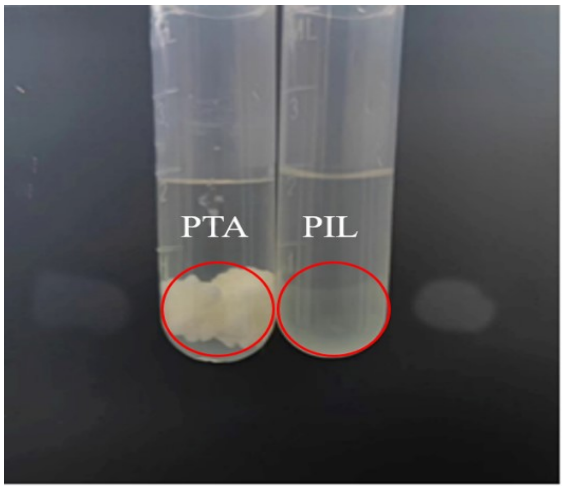

Fig. S9. Comparison of swelling of PIL and PTA in acetonitrile.

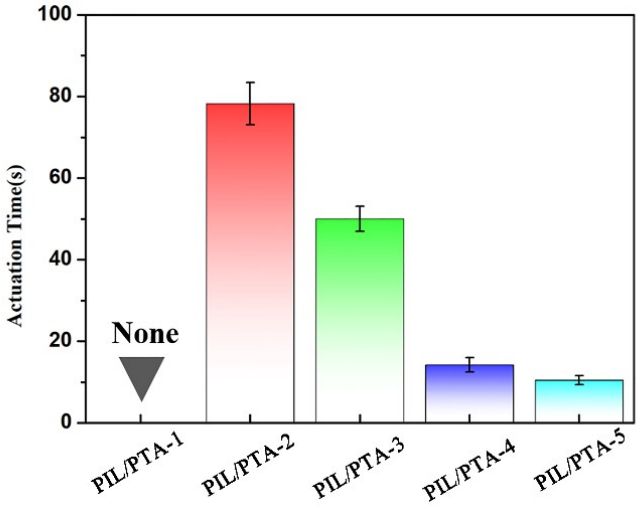

Fig. S10. The acetone actuation performance of PIL/PTA membranes. (No deformation of PIL/PTA-1 film in acetone solvent for any length of time).

Table S2. Summary of the bending performance of PIL/PTA membranes.

Sample	Thickness /mm	Curvature [a] /mm^{-1}	Curvature× Thickness	Time/s
PIL/PTA-1	0.223	0	0	9
PIL/PTA-2	0.230	0	0	9
PIL/PTA-3	0.225	0	0	9
PIL/PTA-4	0.233	0.113	0.0264	9
PIL/PTA-5	0.236	0.209	0.0494	9

[a] The curvature is calculated according to the following procedure, the calculated curvature is up to the bending angle at 9 s. r and curvature can be calculated by the following equation: r = (180L/θπ), Curvature = 1/r. Where L is the length of the membrane (mm); θ and r is the center angle and radius of the curved membrane.[2]

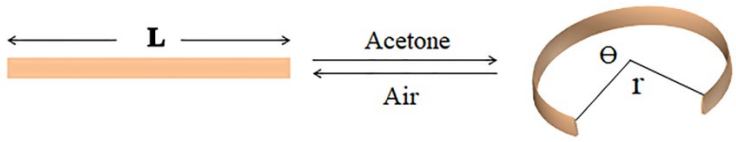

Table S3. Bending properties in the present work and previous literature results. Note: consider a unidirectionally curved actuator. Within each cited paper, we chose the fastest speed for comparison.

Entry	Time/ s	Curvature ×thickness	Ref.
1	9	0.05358	This work
2	0.4	0.0402	*Nat. Commun.* **5,** 4293 (2014)
3	0.5	0.00488	Angew. Chem. Int. Ed. 52, 10482-10486 (2013)
4	1	0.00459	J. Am. Chem. Soc. 133, 15810-15813 (2011)
5	1	0.00174	Angew. Chem. Int. Ed. 51, 4117-4121 (2012)
6	1	0.00556	Adv. Mater. 21, 1582-1585 (2009)
7	2.5	0.003	ACS Appl. Mater. Interfaces 4, 6552-6559 (2012)
8	3	0.00175	J. Am. Chem. Soc. 132, 14172-14178 (2010)
9	3	0.00756	Chem. Mater. 14, 2546-2552 (2002)
10	3	0.01417	Sensors and Actuators A (Physical) 130-131, 1-11 (2006)
11	4	0.01183	Mater. Chem. 20, 7123-7130 (2010)
12	4.5	0.00333	Adv. Mater. 23, 4312-4317 (2011)

Entry	Time/ s	Curvature ×thickness	Ref.
13	5	0.01364	Soft Matter 6, 3447-3449 (2010)
14	5	0.00267	ACS Appl. Mater. Interfaces 3, 4190-4196 (2011)
15	5	0.017	Comput. Chem. 26, 1701-1718 (2005)
16	5	0.00011	ACS Nano 6, 4508-4519 (2012)
17	5	0.0162	Polymer 49, 5520-5525 (2008)
18	6	0.0314	ACS Appl. Mater. Interfaces 9, 15148−15155 (2017)
19	10	0.02186	Appl. Polym. Sci. 127, 2670-2677 (2013)
20	10	0.01047	Appl. Phys. 112 (2012)
21	10	0.01049	Biomacromolecules 9, 1208-1213 (2008)
22	10	0.02356	Biomacromolecules 11, 3638-3643 (2010)
23	10	0.01586	Eur. Polym. J. 49, 1871-1880 (2013)
24	13	0.02043	Sensors and Actuators a-Physical 126, 173-181 (2006)
25	15	0.00414	ACS Appl. Mater. Interfaces 5, 4945-4950 (2013)
26	15	0.03953	Soft Matter 7, 7231-7239 (2011)
27	20	0.00267	Langmuir 26, 16634-16637 (2010)
28	20	0.00119	Mater. Chem. 19, 3141-3143 (2009)
29	20	0.02516	Macromolecules 36, 2055-2065 (2003)
30	30	0.01033	Adv. Funct. Mater. 18, 1290-1298 (2008)
31	30	0.03141	Phys. Chem. B 109, 14789-14791 (2005)
32	32	0.00183	Mater. Chem. 15, 5043-5048 (2005)
33	50	0.001	ACS Nano 4, 6050-6054 (2010)
34	56	0.00146	Chem. Mater. 21, 898-902 (2009)
35	60	0.02967	Polymer 52, 2430-2436 (2011)
36	60	0.01754	Polymer 53, 3677-3686 (2012)
37	100	0.00995	Electrochim. Acta 53, 5555-5562 (2008)
38	120	0.01848	Chem. Mater. 16, 2499-2502 (2004)
39	120	0.00892	Nat. Commun. 4, 2208 (2013)
40	120	0.00268	Mater. Chem. 22, 13473-13476 (2012)
41	120	0.01047	Polym. J. 42, 1609-1616 (2006)
42	200	0.01745	Appl. Polym. Sci. 91, 3613-3617 (2004)
43	300	0.02183	Polym. Adv. Technol. 23, 1234-1239 (2012)
44	390	0.0003731	Appl. Polym. Sci. 113, 1330-1334 (2009)
45	600	0.00426	Mater. Chem. 20, 7123-7130 (2010)
46	750	0.01163	Appl. Polym. Sci. 107, 391-395 (2008)
47	900	0.00321	Soft Matter 5, 308-310 (2009)

Fig. S11. PIL/PTA-5 membrane mimics mimosa response to external stimuli.

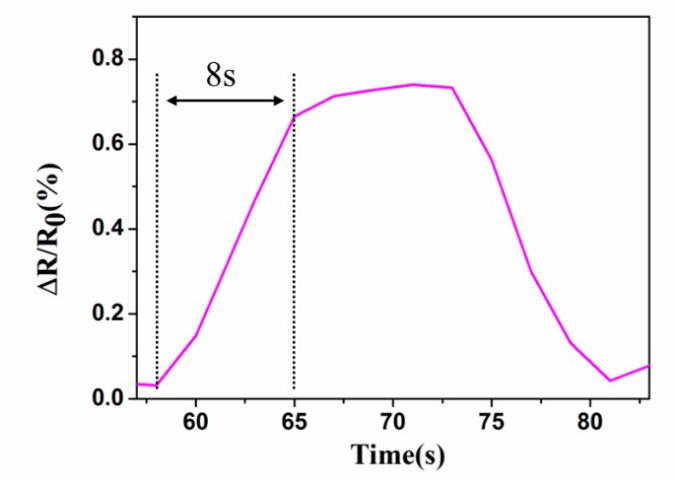

Fig. S12. Response time variation of relative resistance during a solvent sensing test.

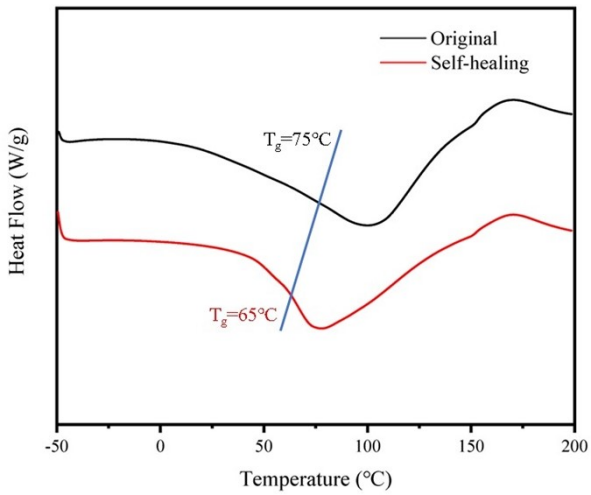

Fig.S13. T_g of PIL/PTA-5 membrane before and after self-healing

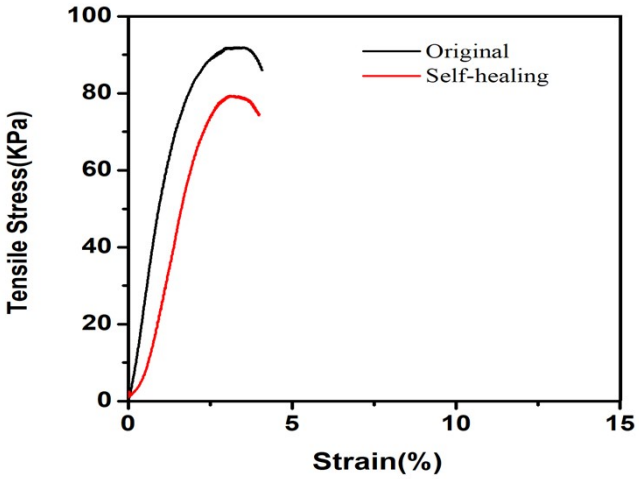

Fig. S14. Stress−strain curves of PIL/PTA-5 membrane before and after self-healing.

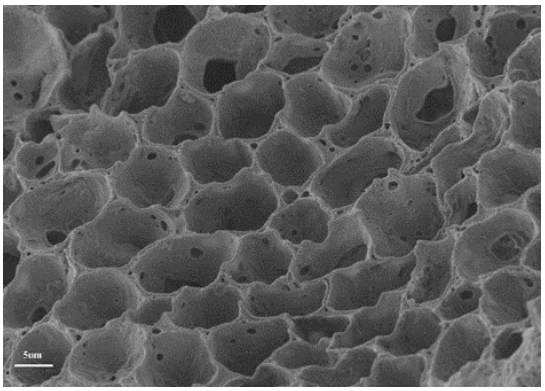

Fig. S15. SEM images of PIL/PTA-5 membrane cross-sections after 10 actuation cycles.

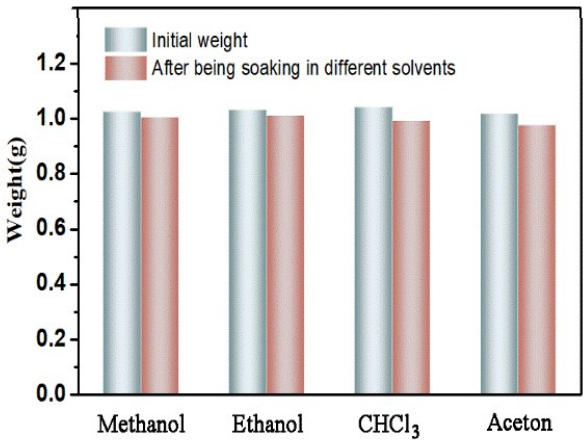

Fig. S16. Weight variation of PIL/PTA membranes after immersion in different organic solvents for 24 h.

References

[1] Y. Shao, Z. Jiang, Y. Zhang, T. Wang, P. Zhao, Z. Zhang, J. Yuan, H. Wang, *ACS Nano,* 2018, **12** (11), 11704-11710.

[2] Q. Zhao, J.W.C. Dunlop, X. Qiu, F. Huang, Z. Zhang, J. Heyda, J. Dzubiella, M. Antonietti, J. Yuan, *Nat. Commun.,* 2014, **5** (1), 4293.